Optimised corrections for finite-difference modelling in two dimensions

Peter M. Manning and Gary F. Margrave

ABSTRACT

Finite-difference two-dimensional correction filters were designed by least squares optimisation in the frequency domain. It is shown how these spatial convolution filters improve responses within a specified frequency range, with the constraint of a limited size. Examples are used to show the improved modelling results, with displays in the wavenumber and spatial domains. The superiority of this method is also shown by a direct comparison with the established Levander method, which uses a split step and fourth order accurate spatial derivatives.

INTRODUCTION

Finite-difference modelers have always been limited by the fact that although frequencies in their data may be represented right up to the Nyquist frequency, the accuracy of the amplitudes at even small fractions of Nyquist degrades when they are used for modelling. Many methods have been used to enhance the accuracy of modelling results at higher frequencies. These include pseudo-spectral methods (Kreis and Oliger 1972) and use of higher order derivative methods (Levander 1988). These methods all effectively use larger operators in the spatial domain to improve the accuracy of the finite-difference derivatives, however, they do not address the accuracy of the temporal derivative other than to take small time steps. We have suggested use of correction operators, that correct for both space and time finite-differences, designed in the wavenumber-domain (Manning and Margrave 2000), and there we applied the corrections in that domain. In this paper we show how these wavenumber-domain operators may be made into spatial operators of practical sizes when the range of the desired 'flat' frequency response is not too large (for example, to one half the Nyquist wavenumber).

OPTIMUM SPATIAL DESIGN

We have found that much improved frequency responses may be obtained with quite small operators, and small operators are an advantage because the problems with internal boundaries and edges are reduced. We have also found it practical to design these operators within an inherently stable choice of sample rates. This means that generally the higher the frequency, the more its amplitude must be enhanced, but frequencies above the design window may be left attenuated.

We develop the method by beginning with a one-dimensional transform in matrix form, and then use this form to obtain a limited length filter with optimal frequency response. This is a straightforward process. The two-dimensional transform case may then be developed by analogous means, although the matrix manipulations are a bit unusual. Some of the Fourier transform matrices are represented in figures in analogue form, which makes the explanation more intuitive.

The one spatial dimension case

The one dimensional Fourier transform may be represented in matrix format as shown in Figure 1. The lower frequencies (only cosines are shown, sines are done in similar fashion) are represented along rows in analogue fashion within the matrix. The equation shows how these row samples representing a single frequency are multiplied by the data samples and summed to give the amplitude of each frequency in the transformed vector.

Figure 2 shows the case where the data vector is all zeros past a given point. It may also represent the case where, beyond a certain point, the data is unknown and hopefully won't contribute much to the spectrum. In this case a transform may still be found, but the cosine curves within the transform matrix may be cut off to the data length, as shown in the figure. The equations represented in Figures 1 and 2 may be represented in algebraic form by the equation

$$MV = T\,, \tag{1}$$

where M is the Fourier transform operator matrix, V is the data vector to be transformed, and T is the transformed result.

The case in which we are interested is shown in Figure 3. It is identical to Figure 2 except that the frequency response is given, and the data vector is now an unknown filter that we want designed to make the equation work as closely as possible. The matrix equation may be represented by

$$MU \approx D\,, \tag{2}$$

where M is the transform matrix, U is the unknown vector or filter, and D is the desired frequency response. A solution for U can then be found in a least squares sense by applying standard inverse theory. The solution is given by

$$U \approx M^T D\left(M^T M\right)^{-1}, \tag{3}$$

where the superscript T indicates transpose and -1 indicates inverse. Note that if the unknown filter is not truncated, the M^TM matrix is the identity matrix, the inverse is also the identity matrix, and the solution is trivial. When the unknown filter is truncated the Fourier components are not orthogonal, and the solution is not trivial.

The two spatial dimensions case

The two dimensional Fourier transform operates, in this case, on the surface with the independent variables x and z, and is transformed into the surface with the independent variables specified as the x and z wavenumbers. A four dimensional matrix may be set up to do this transform.

In Figure 4, a pseudo matrix equation to obtain a few of the lower frequency two dimensional Fourier coefficients is shown. This is analogous to the one dimensional equation in Figure 1. The four dimensional transform matrix has been specified here as the matrix of matrices shown on the left. Next to it is the input spatial data set, and to the right of the equal sign is the output data set. The transform is done by overlaying each

elementary Fourier component matrix (within the super matrix on the left) on the data matrix and multiplying (element-by-element) and summing to obtain a single output cosine term within the matrix on the right side of the equation. Each elementary matrix is labelled by the frequency in x and z, and also by the analogue frequency traces along each edge. We have called this a pseudo matrix equation because each sub matrix acts like a row in the equation in Figure 1. The equivalent 2D Fourier transform for the cosine amplitude $C_{m,n}$ is given by

$$C_{m,n} = \iint Emn(x,z)\,S(x,z)\,dxdz\,, \tag{4}$$

where

$$Emn(x,z) = \left[\cos(2\pi mx)\cos(2\pi nz)\right], \tag{5}$$

the two dimensional function of the cosines multiplied together. This is constructed before multiplication with the data surface S, and the result is integrated (summed).

Figure 5 shows the partial 2D Fourier transform, analogous to Figure 2. This demonstrates the case where the surface (or filter) is limited in size. In practice these matrices will be small, perhaps as small as 3x3, which represents a final filter size of 5x5. The number of these matrices may be large, perhaps containing frequencies up to half of Nyquist, although each frequency is represented by only its leading few samples (in the first case mentioned, only the leading 3 samples).

Figures 6 and 7 show the steps taken to reform the matrices into standard shapes. Figure 6 shows the stage where the elementary Fourier matrices have been resized into long row vectors, and the surface has been resized into a long column vector. This reshaping is legitimate as long as it has been done consistently, with the same pairs of numbers multiplied together before adding to the same sum.

Figure 7 shows how the matrices have been resized into a standard matrix equation format. At the same time, analogous to the difference between Figures 2 and 3, the equal sign has been changed into an approximation sign to indicate that the column vector on the right is the known (desired) response, and the column vector which is part of the matrix multiplication is the unknown filter. This fits the format of equation (2), which has the solution given by equation (3). This solution is a vector which may be resized in reverse fashion into a 2D filter with a least squares optimal frequency response.

In practice, the elementary matrices shown in analogue form are modified slightly to represent the analysis of a two dimensional filter that is zero phase in both directions. The Fourier components may be obtained from little more than one quarter of the values in a filter of this type, and they are guaranteed to be all cosines, but the coefficient matrices must be modified to allow for the duplicated samples in the other three quadrants.

Design Examples

The section following this one compares the Levander finite-difference scheme and the correction filter as optimised by the technique described above. Some of the figures from this section are good examples of the design techniques described here.

One set of comparisons shows the wavenumber response of individual terms of the wave equation. The ideal responses are from the ratios of sinc functions by which the theory was developed. These may be compared to the filters defined in space that are 5 by 5 in total size, and then to the filters that are 9 by 9 in total size. These filter sets are both optimized in the wavenumber domain from zero to ½ Nyquist.

In the last row of the table, Figures 21 and 22 show the total effect of complete sets of 5 by 5 and 9 by 9 corrections on a model after 100 steps. The smaller ring is pure shear, and the larger ring is pure compressional energy.

	COMPARISON	5 BY 5	9 BY 9
$\frac{\partial^2 U_z}{\partial z^2}$	Figure 9 (ideal)	Figure 11	Figure 12
$\frac{\partial^2 U_x}{\partial x \partial z}$	Figure 13 (ideal)	Figure 15	Figure 16
Model	Figure 19 (uncorrected)	Figure 21	Figure 22

Comparison of the individual term response in the wavenumber domain shows the expected results of a better fit with a larger pattern. It seems a bit surprising that the 5 by 5 terms are as good as they are. However, the 9 by 9 terms are a little better within the design zone, and significantly better just beyond it. This probably results from the fact that the slopes near the edge of the design zone are represented more accurately. It is not yet clear which effect causes more of the improvement of the correction.

Comparison of the practical modelling results in Figures 19, 21 and 22 shows significant improvement with the smaller spatial operator, and even more with the larger operator. The smaller operator brings the large ring of the pressure wave much closer to the zero phase character of the initial wavelet, and brings the small ring of the shear wave into a circle. The larger operator brings the pressure wave to zero phase, and the shear wave is made more compact and shows its zero phase character as well.

OPTIMUM DESIGN VS 4TH ORDER DERIVATIVES

This section compares the effects of the correction operators shown above, and the fourth-order second derivatives used in (for example) Levander (1988). Both systems (and others) ultimately use an extended set of sample points in space (extended beyond that required for the minimal 3-pt second-derivative approximations) to obtain more accurate modelling results. The method used will be to restrict the correction operator in space to the same extended number of samples required for the fourth order operators,

and compare results. The cases of uncorrected modelling and longer correction operators will also be shown.

The Levander modelling scheme

The Levander scheme uses a split time step system, where the second-order wave equation is split into two first-order equations, and each of these equations is stepped through a time interval of one-half of the time sample rate. It also uses a higher order approximation for the continuous spatial derivatives. Instead of using the first-order operator of [1,-1] for a derivative, the operator [-1/24, 9/8, -9/8, 1/24] is used for each of the two steps. For comparison purposes, we consider this to be the first order operator convolved with a correction filter of [-1/24, 13/12, -1/24].

The correction filters are effectively applied to both stages of the split-step process, and so the complete second-derivative corrections are a combination of two stages of the first-order corrections. The equivalent correction in the direction of the axes (either *x* or *z*) is [1/576, -13/144, 113/96, -13/144, 1/576]. The equivalent correction for the cross-term calculations is a symmetric square function,

$$\begin{bmatrix} \frac{1}{576} & -\frac{13}{288} & \frac{1}{576} \\ -\frac{13}{288} & \frac{169}{144} & -\frac{13}{288} \\ \frac{1}{576} & -\frac{13}{288} & \frac{1}{576} \end{bmatrix}. \qquad (6)$$

The first type of operator is the longest at 5 points, requiring two extra points in each direction for the correction to be effective. This must be considered near any boundaries because the extra input points are required in both the *x* and *z* directions.

Figure 8 shows all of the displacements used as input points for the Levander acceleration in *z*. The $\partial^2 U_z / \partial z^2$ term has input from the column of *z* displacements. The $\partial^2 U_z / \partial x^2$ term has input from the row of *z* displacements, and the $\partial^2 U_x / \partial x \partial z$ term has input from all of the *x* displacements shown. In contrast, the second order derivatives plus optimum corrections developed in this paper use an array of points for every term that contributes to the acceleration.

Examples of Levander and correction filter effectiveness - wavenumbers

The cases here all have spatial sample rates of 6 metres. These presentations are all in the wavenumber domain, where the enhancement contour levels must be compared to judge effectiveness. A quarter circle centred on the zero wavenumbers is marked because this is the zone where the response was optimized using equation 3, and with the matrices developed as in Figure 7. The functions should be compared in this zone, covering an area from the origin to halfway to the Nyquist wavenumbers in each direction.

The first case presented is for the second derivative in the *z* direction of the *z* displacement. The ideal correction is shown in Figure 9, where a pressure wave velocity

of 2000 and a time sample rate of .001 have been specified. The Levander fourth order correction multiplier term is shown in Figure 10. This operator is one column of 5 rows, and appears to be a rough match to the ideal case.

The optimised operators for the case, developed from the theory of this paper, are shown in Figures 11 and 12. The designs match quite closely the zone within the marked quarter circle. The operator of size 5 by 5 was chosen to use the same number of extra points required by the collection of Levander operators. It obviously matches the details of the ideal enhancement much more closely than does the Levander operator. The 9 by 9 sized operator is an even better match, although it will require more extra points beyond any boundaries.

The second case presented is for the second derivative of either the x or z component with respect to both x and z. The ideal correction multiplier term is shown in Figure 13. The Levander correction term is shown in Figure 14, and it has the nearly circular form of the ideal case. The 5x5 operator designed for the same case is shown in Figure 15, and can be seen to have a shape closer to the ideal. The operator designed for the 9 by 9 size has the response shown in Figure 16, and has an even better fit at the larger wavenumbers.

The last case presented is for the second derivative in the z direction of the x displacement. The ideal correction-multiplier term is shown in Figure 17, where the relevant shear velocity of 1000 and a time sample rate of .001 have been specified. The Levander correction in Figure 10 applies to this case too, because it is determined only by the value of the second derivative. The ideal correction is distinct for this case because it allows for the inaccurate second derivative in time, and is affected by the shear velocity and time sample rate. The optimised operator responses are not shown, but they are good approximations at the lower wavenumbers.

Examples of Levander and correction filter effectiveness – space

The natural test of a modelling system is to apply it under controlled conditions. There, the results after many successive steps will show if the small errors of each step are significant enough to accumulate, or by contrast, are a type which tend to cancel out and still give accurate end products. The expanding pressure and shear rings, which are shown at their starting positions in Figure 18, have been found useful for testing the effectiveness of our modelling systems. The two pressure rings both have a zero-phase, symmetric wavelet.

The first test used an uncorrected second order finite-difference modelling program to propagate the rings through 100 steps of .001 seconds each. The output is shown in Figure 19. The numerical dispersion and non circular shape of the smaller shear ring is quite obvious, and the larger pressure ring can be seen to deviate from its original zero phase (symmetric) shape.

The second test in Figure 20 shows the results of the simulated Levander-style wave propagation. The pressure wave has been propagated more accurately as is evidenced by the ring being almost zero phase (symmetric). The shear wave wavelet has been

improved in quality but the wave front has a more obvious deviation from circular. That the shear wave propagation here is less than ideal is not surprising, since the system was not designed for shear waves.

The next test in Figure 21 shows propagation with the optimised correction operator of size 5 by 5. The pressure ring here is even closer to zero phase. The shear ring is almost perfectly circular and compact, but not zero phase.

The final test in Figure 22 shows the use of the optimised correction operator of size 9 by 9. Both of the rings are circular and almost perfectly zero phase.

Discussion

The superior effects of our optimal corrections may be attributed to a number of reasons, theoretical and practical. The optimal corrections:

- are designed for a specific frequency range.
- consider the distortions on the time side of the equations.
- make use of all the input data points which must ultimately be supplied

CONCLUSIONS

For the same number of points (5x5), our correction operators perform significantly better than the Levander operators. With a 9x9 operator, the performance is better yet.

The modelling system may be further improved by using even larger operators, but more effort is required to provide realistic data points from beyond the edges of each constant velocity area.

REFERENCES

Kreiss, H. O. and Oliger, J., 1972, Comparison of accurate methods for the integration of hyperbolic equations: Tellus **24**, 199-215.

Levander, A. R., 1988, Fourth-order finite-difference P-SV seismograms: Geophysics **53**, No 11, 1425-1436.

Manning, P. M. and Margrave, G. F., 2000, Elastic finite difference modeling with stability and dispersion corrections: CREWES research report, v. **12**, 139-156.

FIGURES

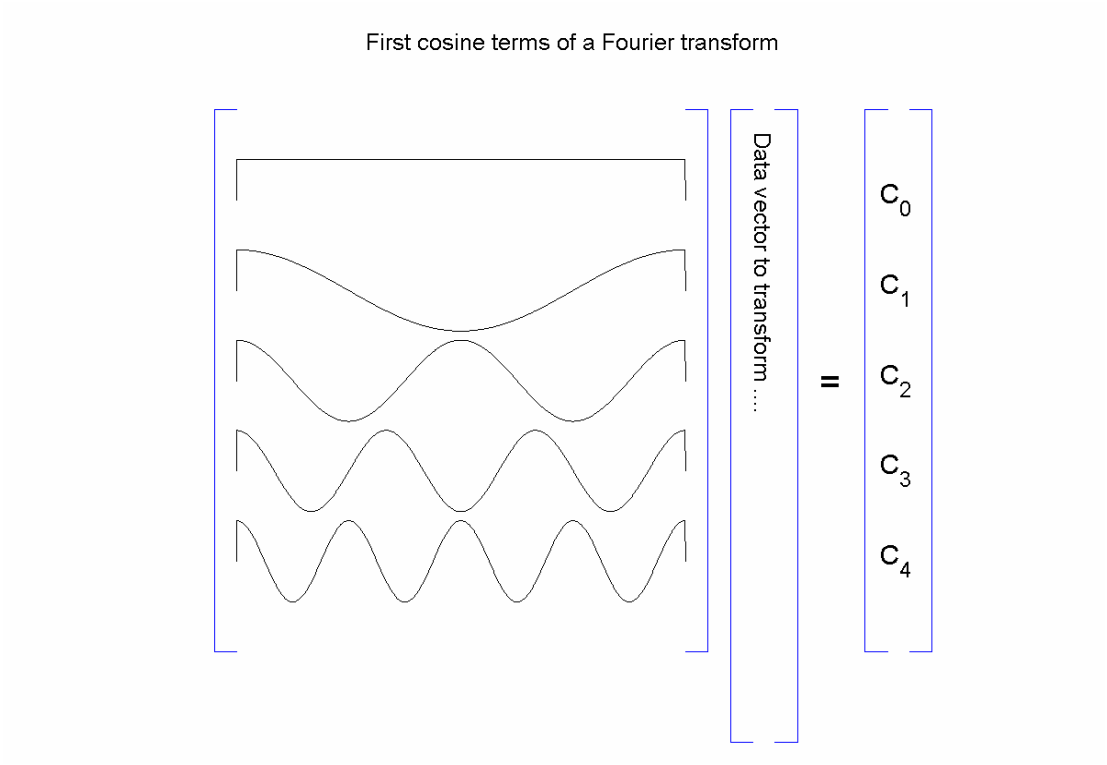

FIG. 1: Fourier transform by a matrix equation (cosines shown).

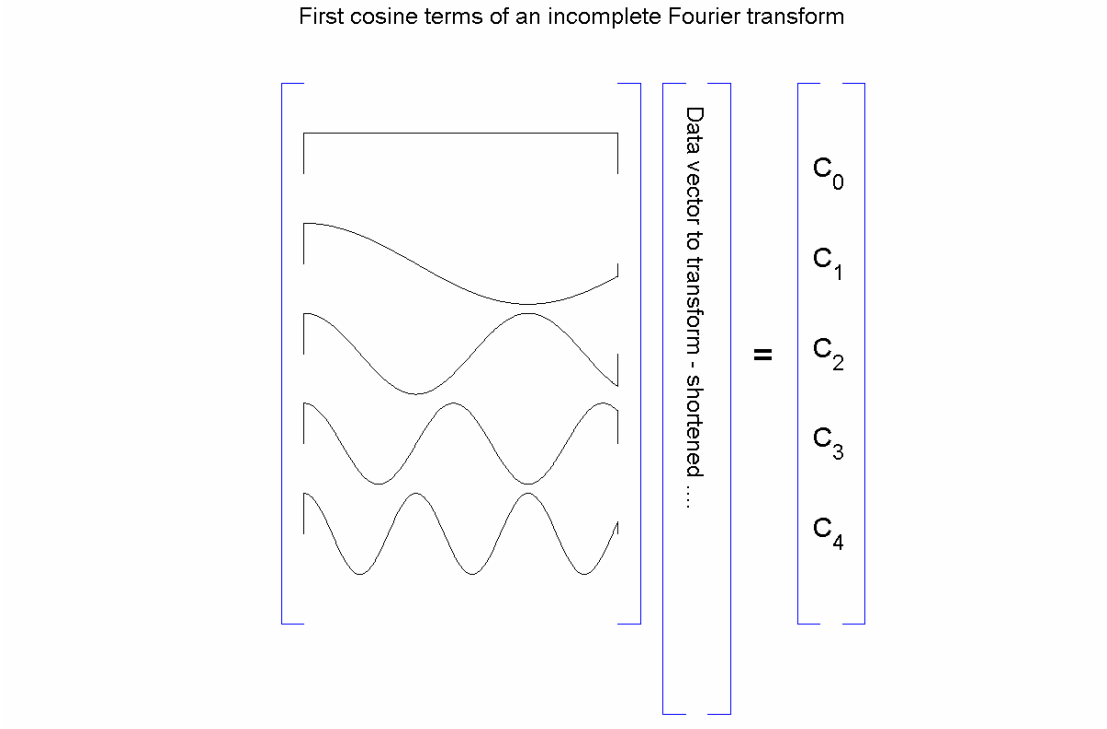

FIG. 2: Fourier transform of a partial (shortened) data vector.

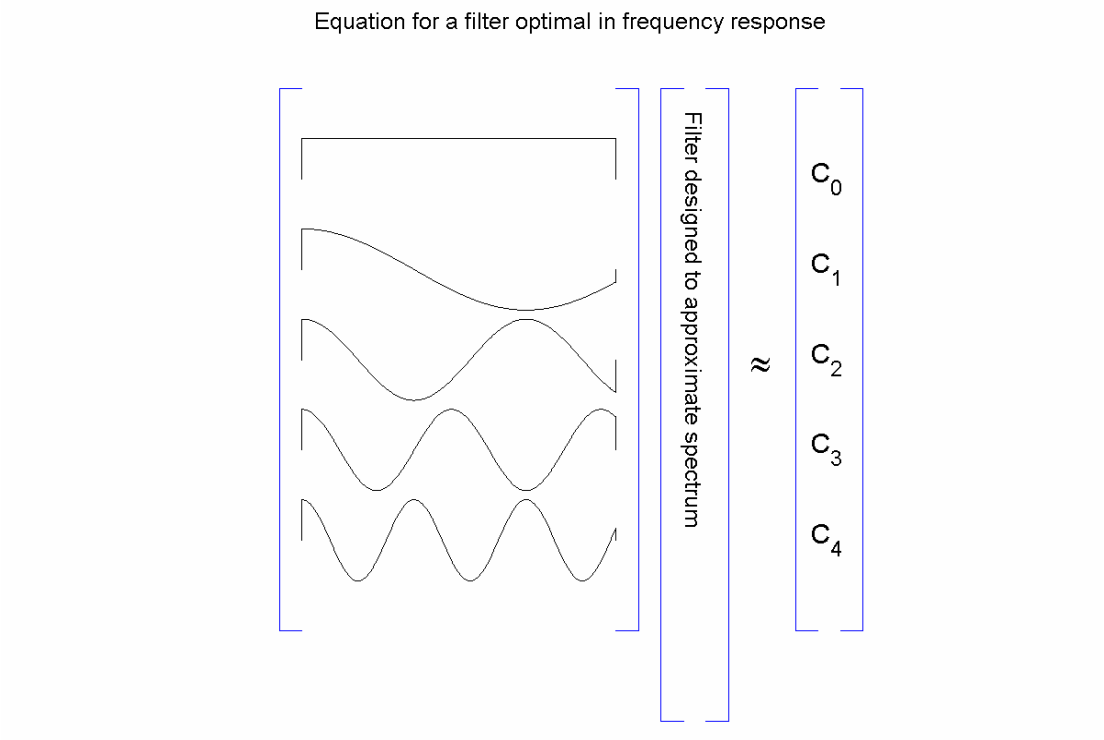

FIG. 3: The matrix equation similar to Figure 2, where the frequencies are specified and the filter must be designed to approximate them

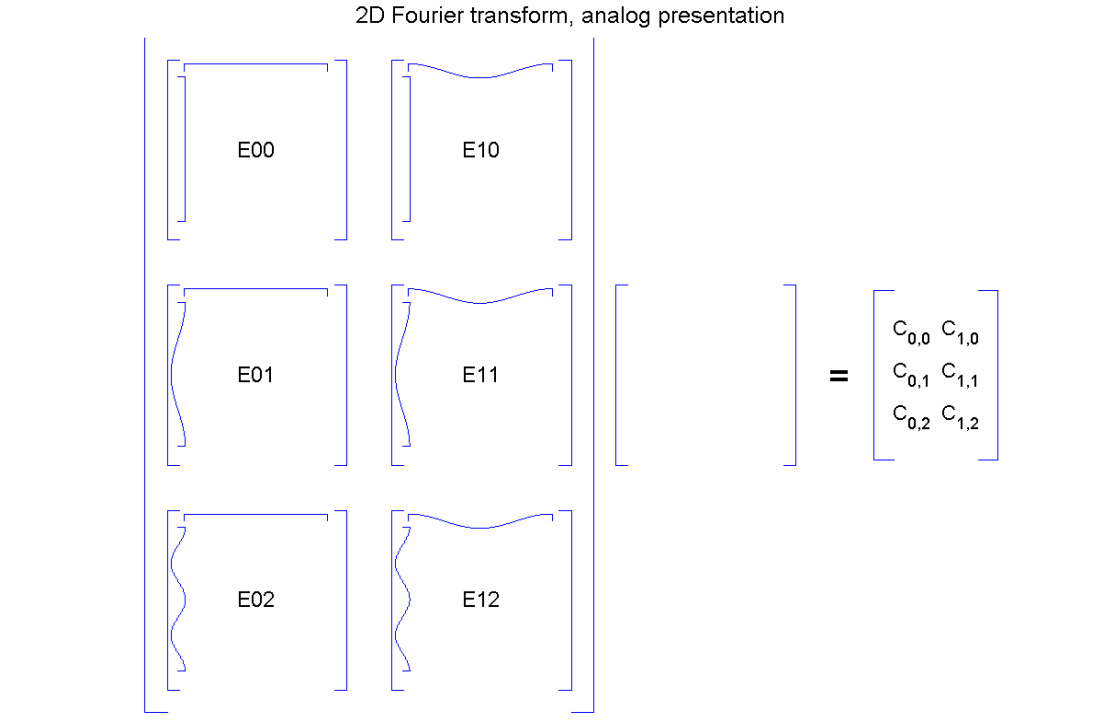

FIG. 4: A 2 dimensional Fourier transform by a matrix equation (cosines shown), an analogue to Figure 1.

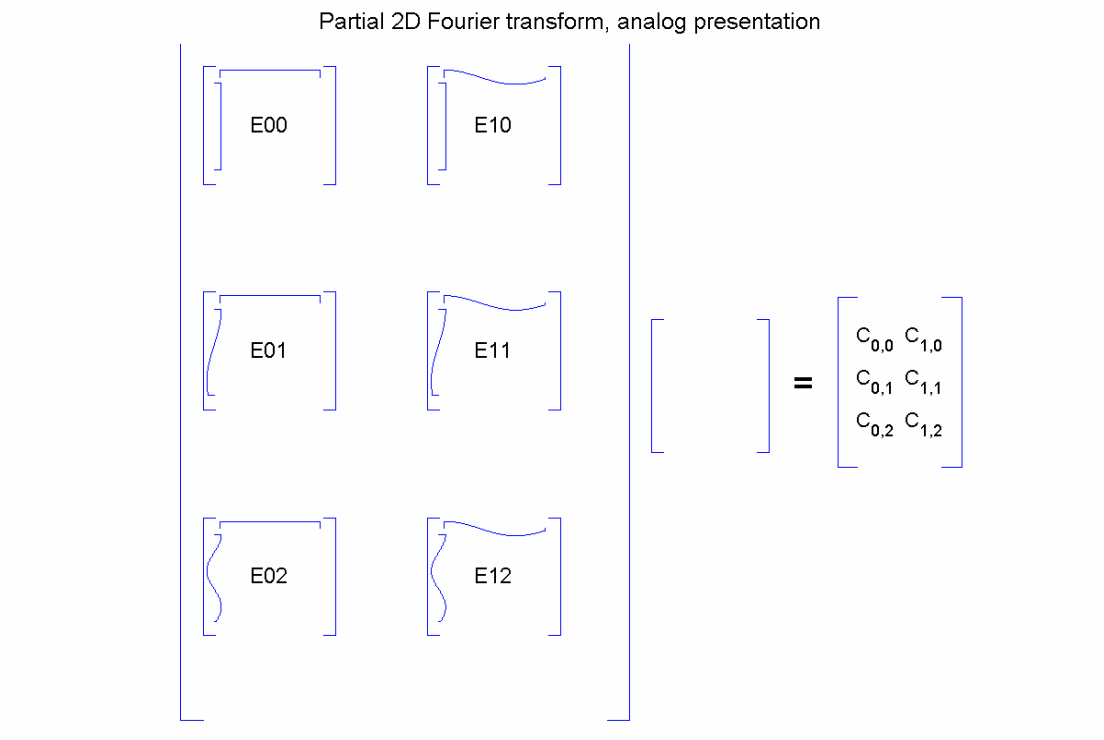

FIG. 5: A 2 dimensional Fourier transform of a partial (length and width reduced) data vector.

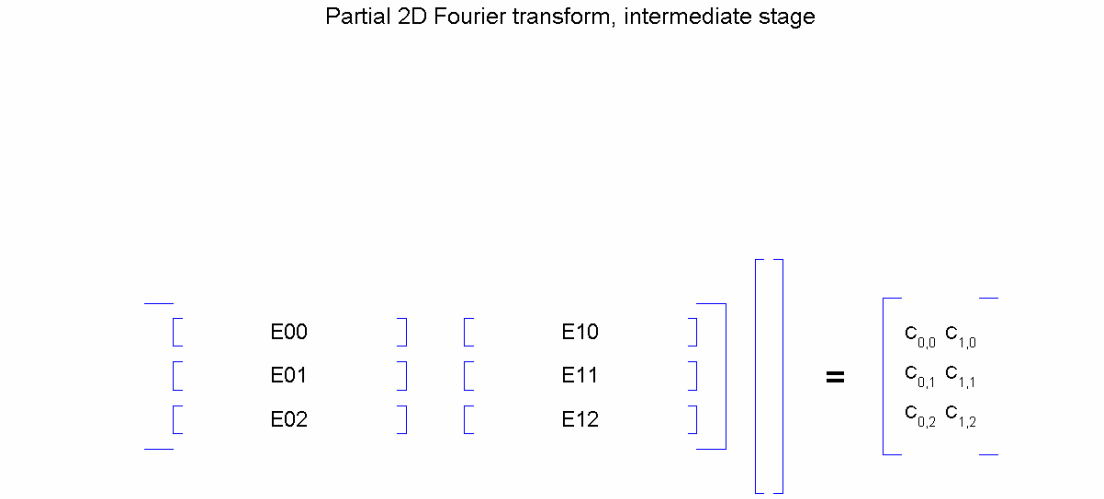

FIG. 6: An equivalent version of the equation shown in Figure 5, with the elementary matrices reformed into rows, and the data into a column.

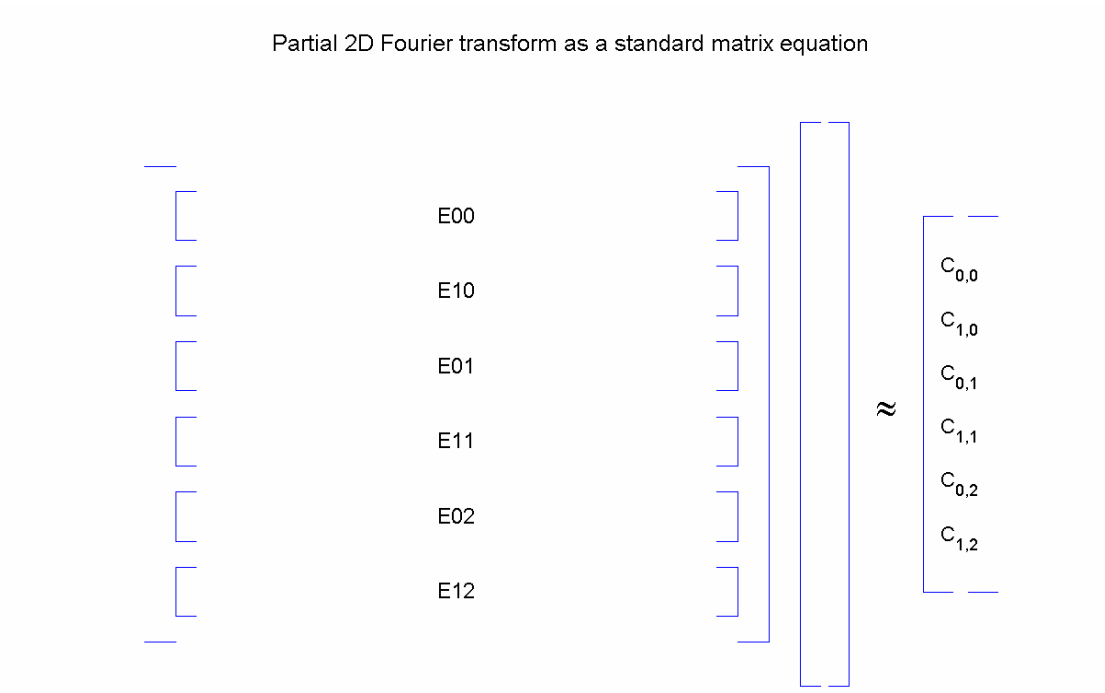

FIG. 7: The equation from Figure 6 has the elementary matrices sorted into separate rows, and output amplitudes reformed into one column. It is in the form $MU \approx D$, analogous to Figure 3.

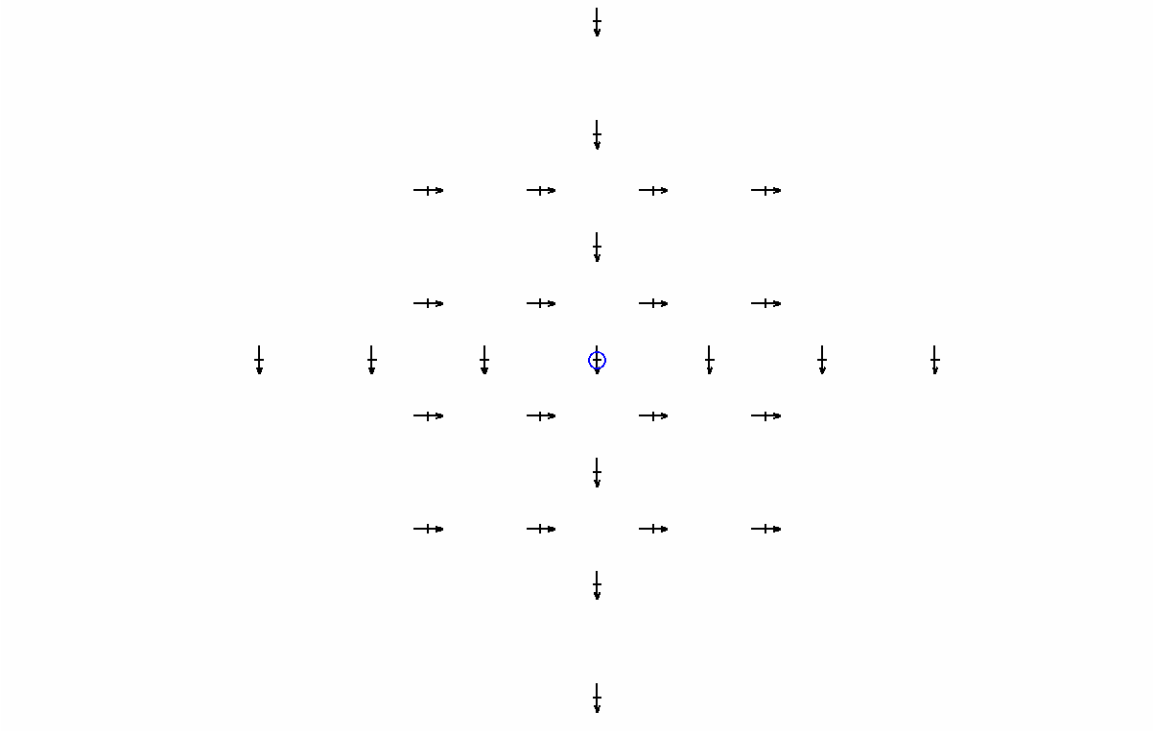

FIG. 8: All the displacements which contribute to the Levander U_z acceleration at the centre.

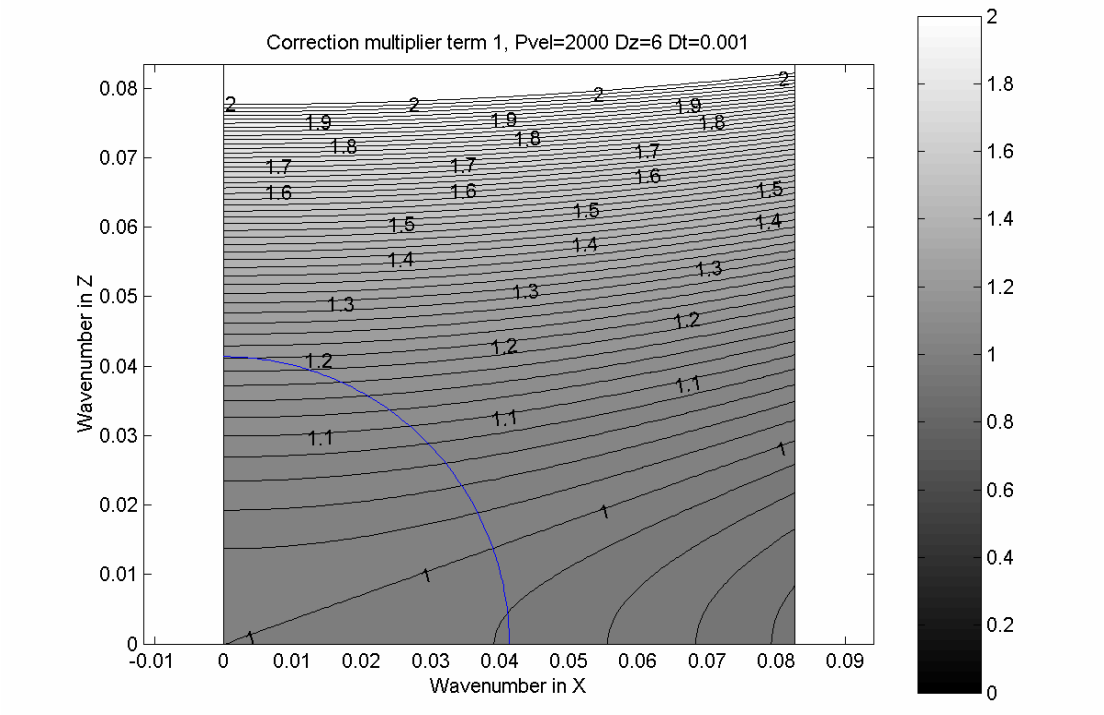

FIG. 9: The ideal correction for the $\partial^2 U_z / \partial z^2$ term.

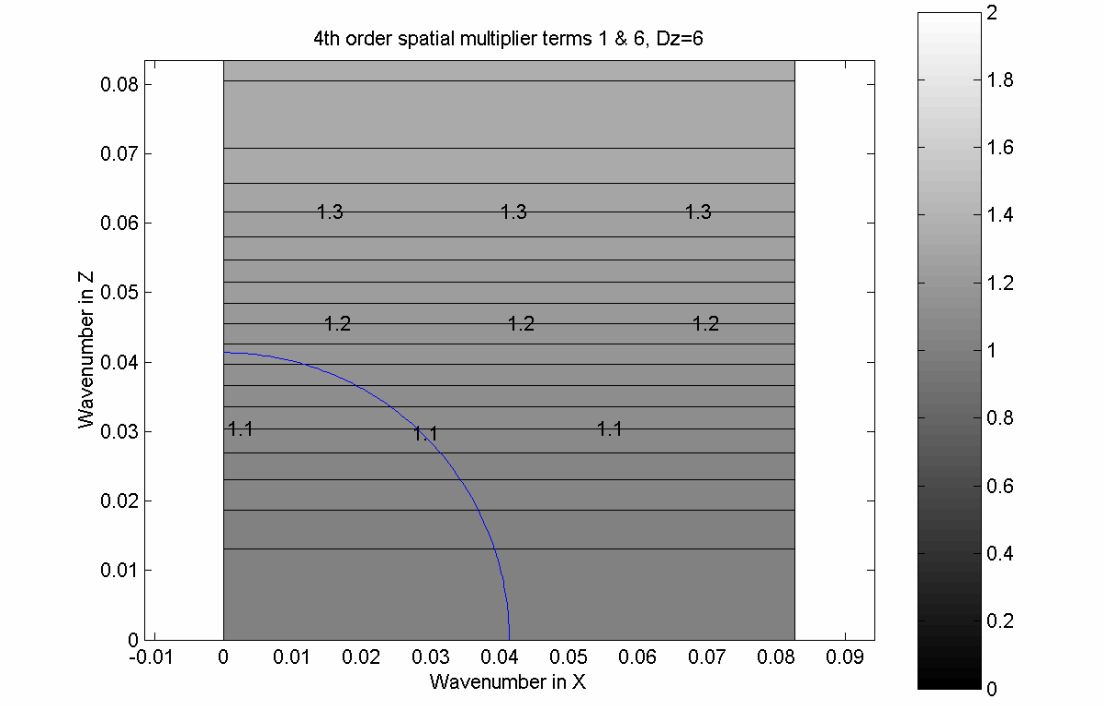

FIG. 10: The fourth order correction for the $\partial^2 U_z / \partial z^2$ term. Compare to Figure 9.

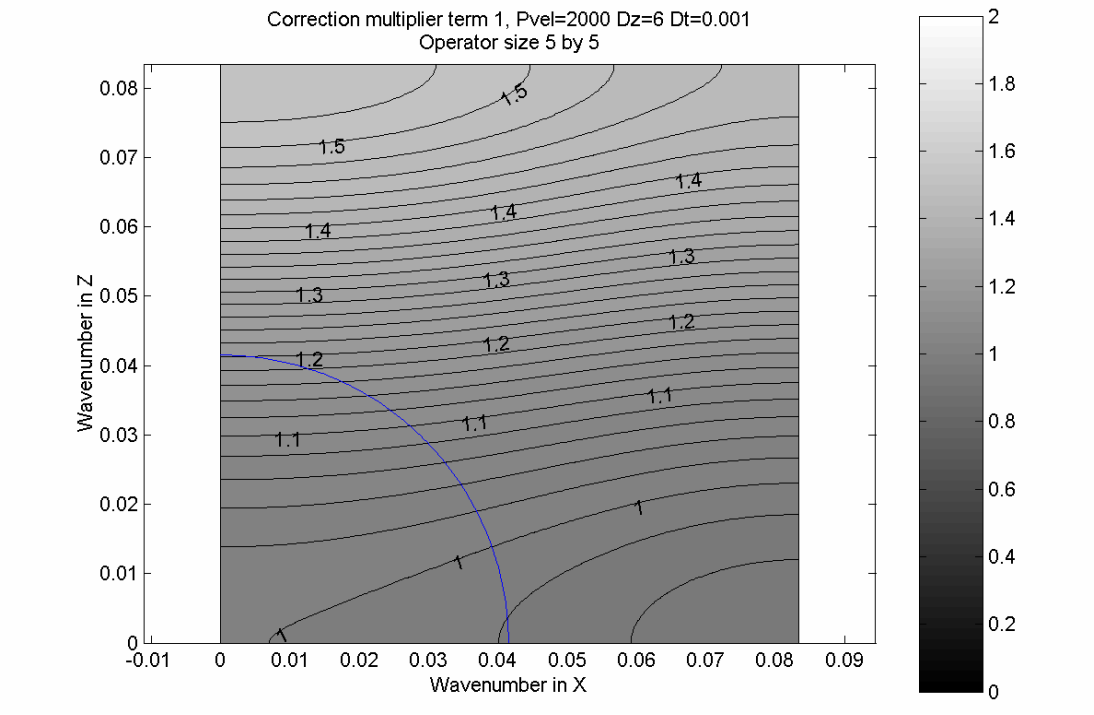

FIG. 11: The optimum 5 by 5 correction for the $\partial^2 U_z / \partial z^2$ term. Compare to Figures 9 and 10.

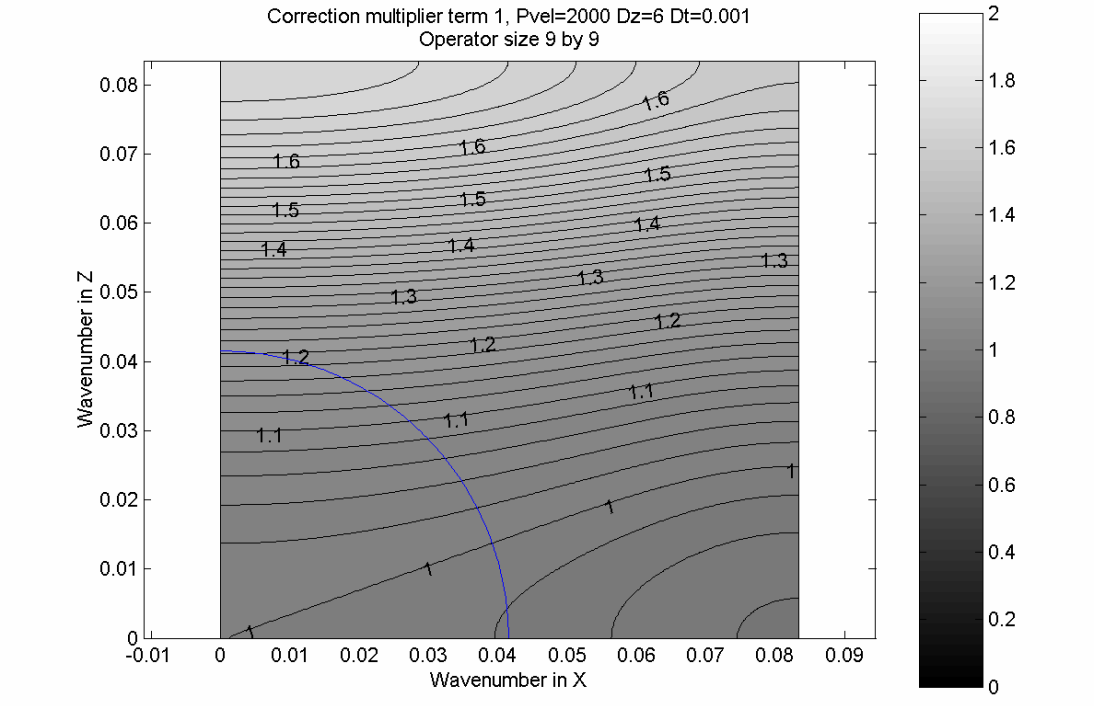

FIG. 12: The optimum 9 by 9 correction for the $\partial^2 U_z / \partial z^2$ term. Compare with Figures 9 – 11.

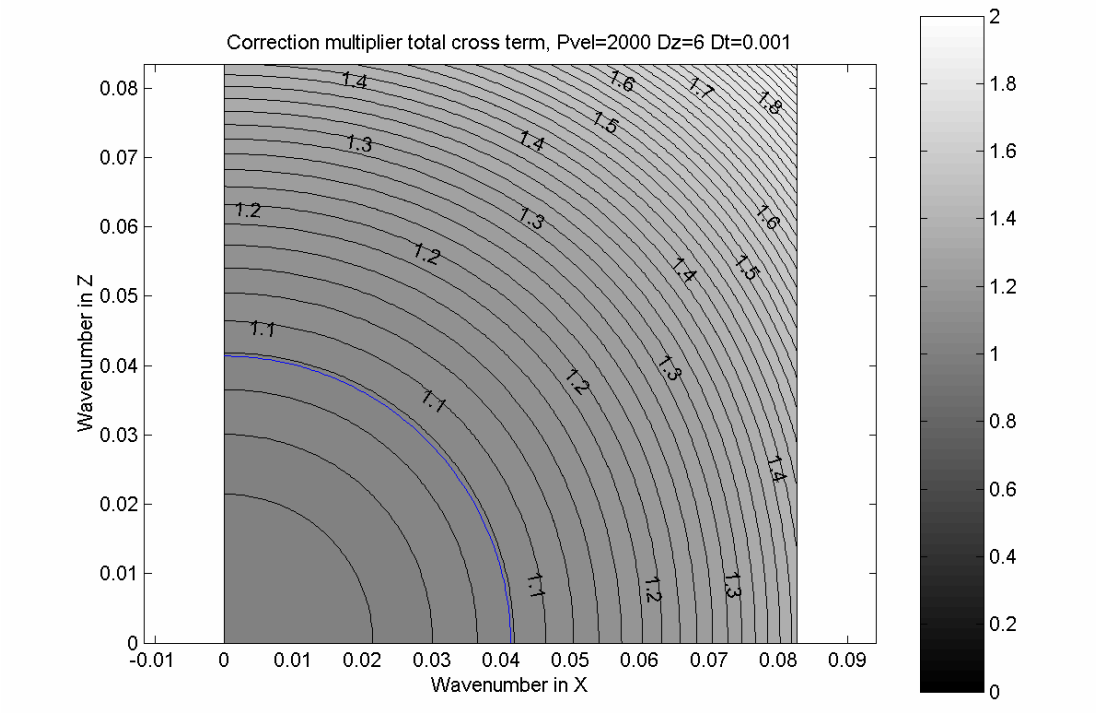

FIG. 13: The ideal correction for the $\partial^2 U_x / \partial x \partial z$ term.

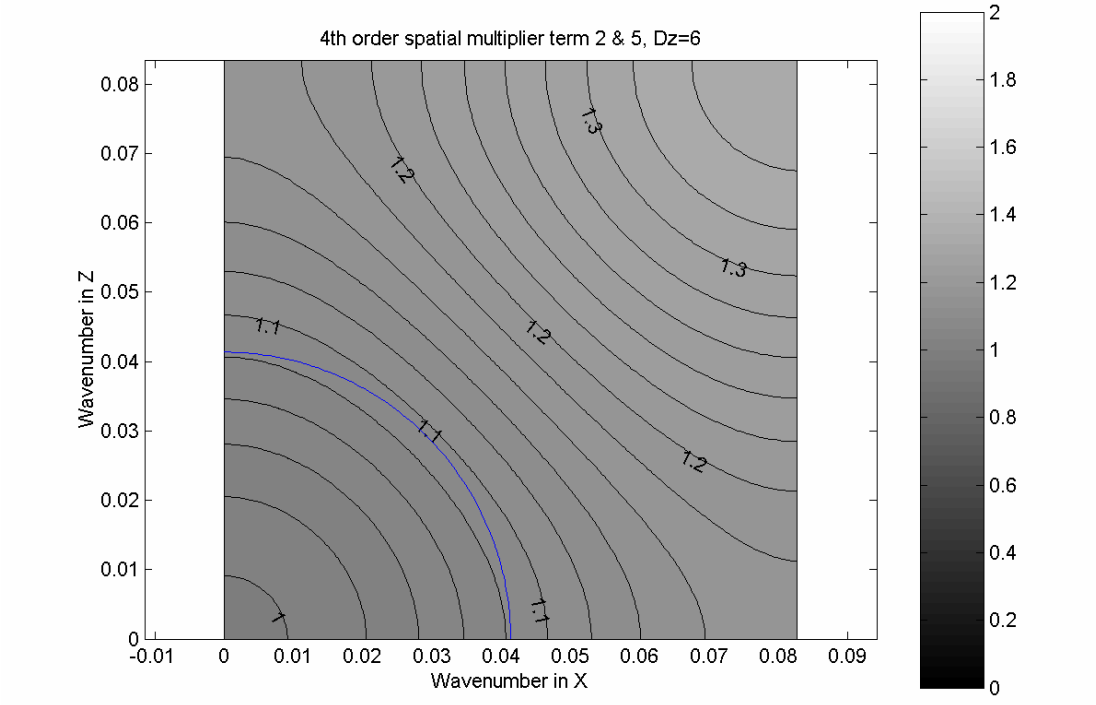

FIG. 14: The 4th order correction for the $\partial^2 U_x / \partial x \partial z$ term. Compare with Figure 13.

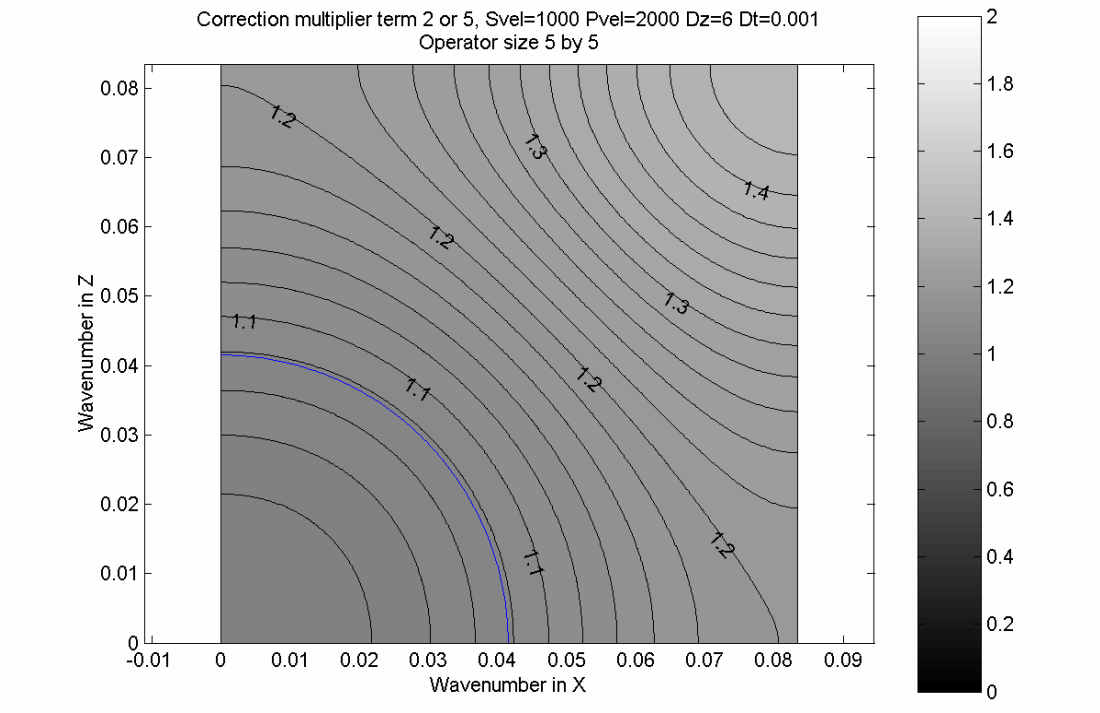

FIG. 15: The optimum 5 by 5 correction for the $\partial^2 U_x / \partial x \partial z$ term. Compare with Figures 13 and 14.

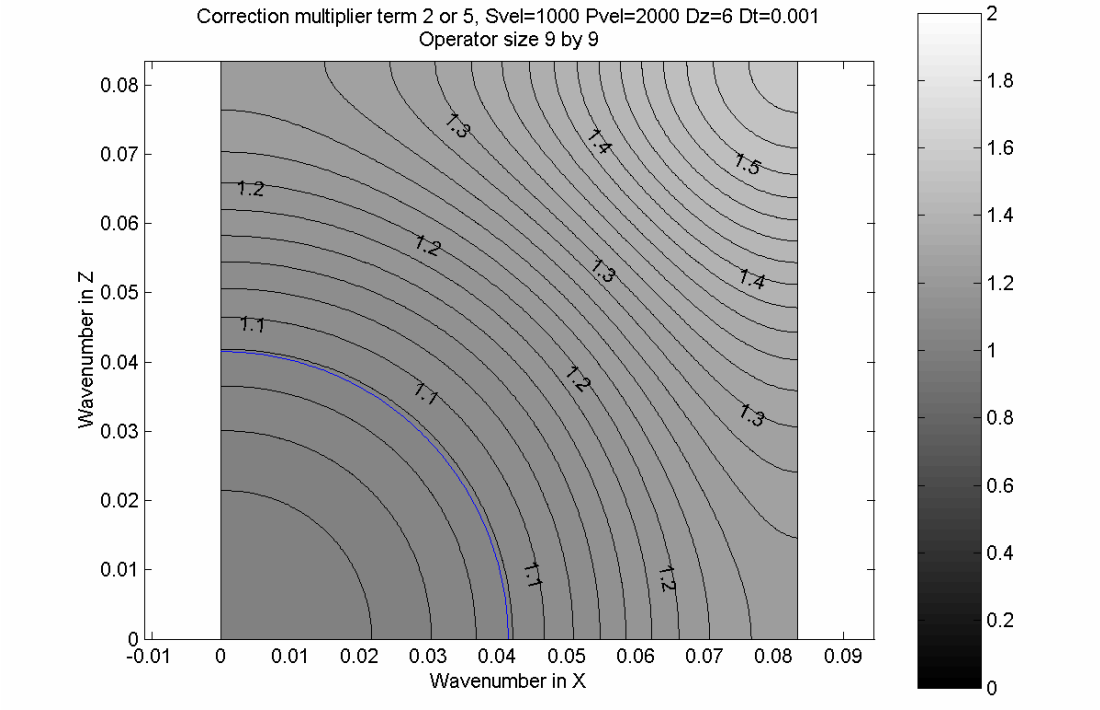

FIG. 16: The optimum 9 by 9 correction for the $\partial^2 U_x / \partial x \partial z$ term. Compare with Figures 13 through 15.

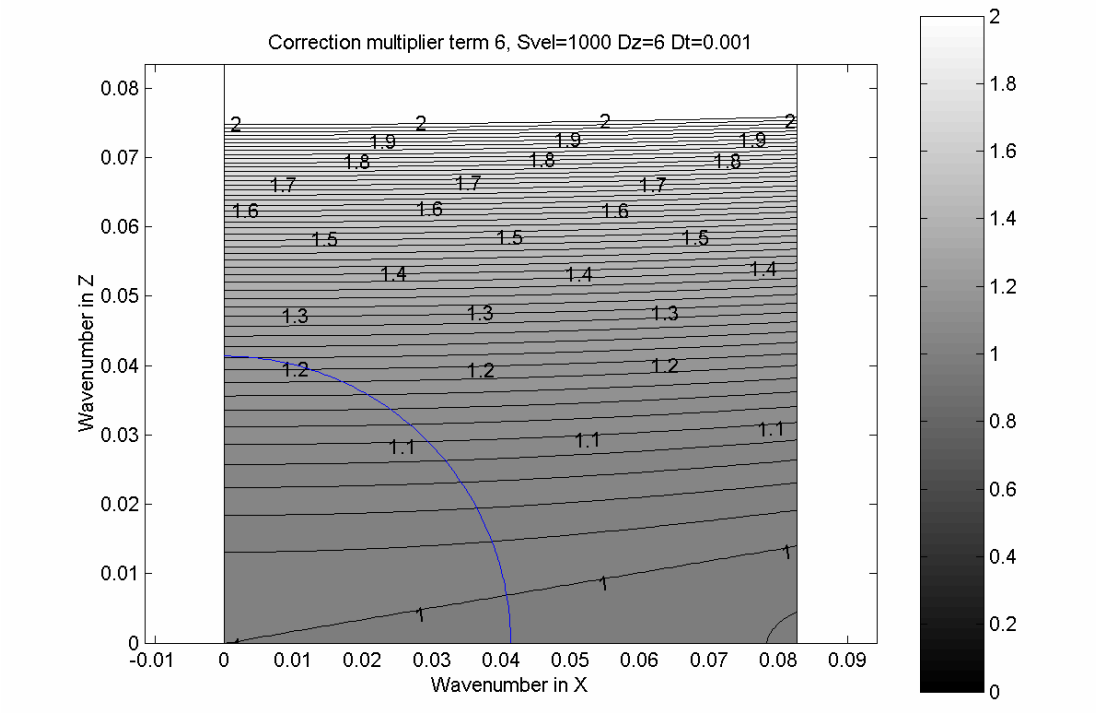

FIG. 17: The ideal correction for the $\partial^2 U_x / \partial z^2$ term. Compare with Figure 10.

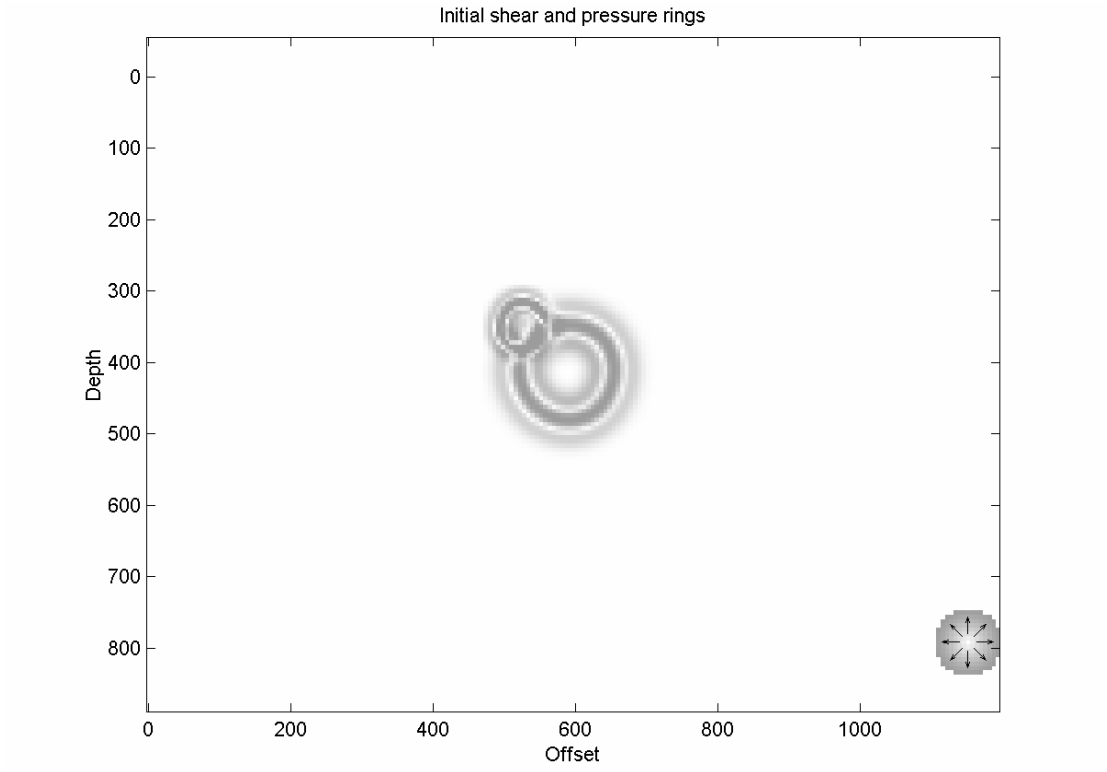

FIG. 18: The initial shear (left) and pressure rings, propagated in Figures 19 through 22.

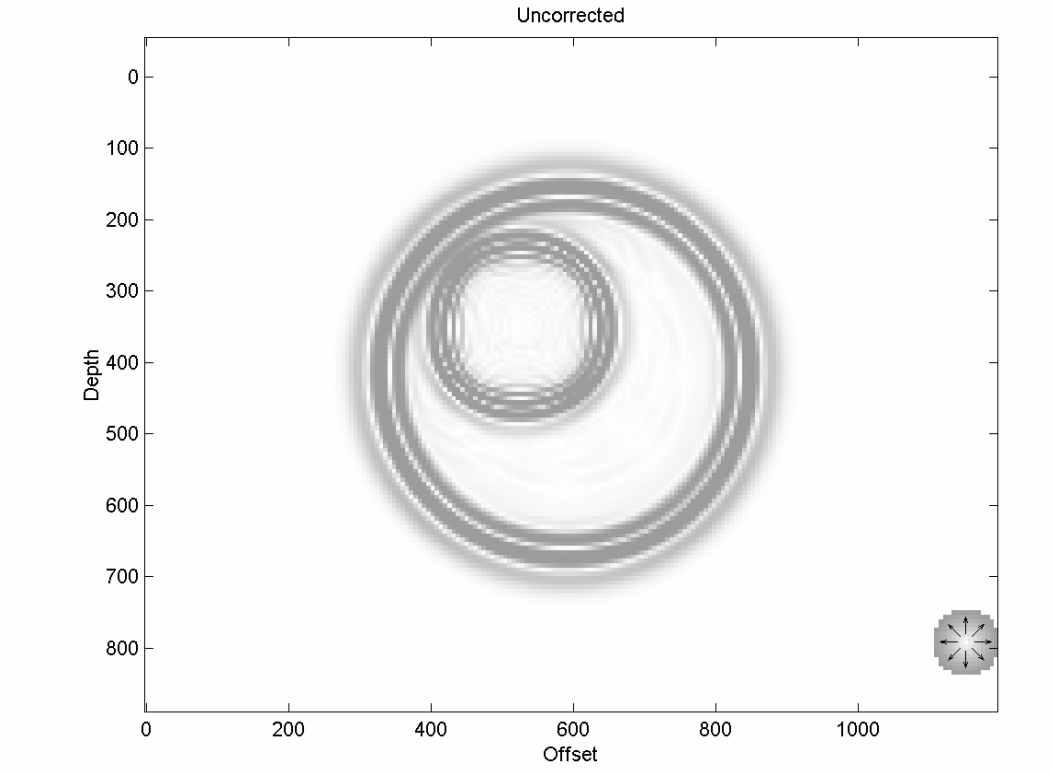

FIG. 19: The uncorrected model after propagation through 100 time steps.

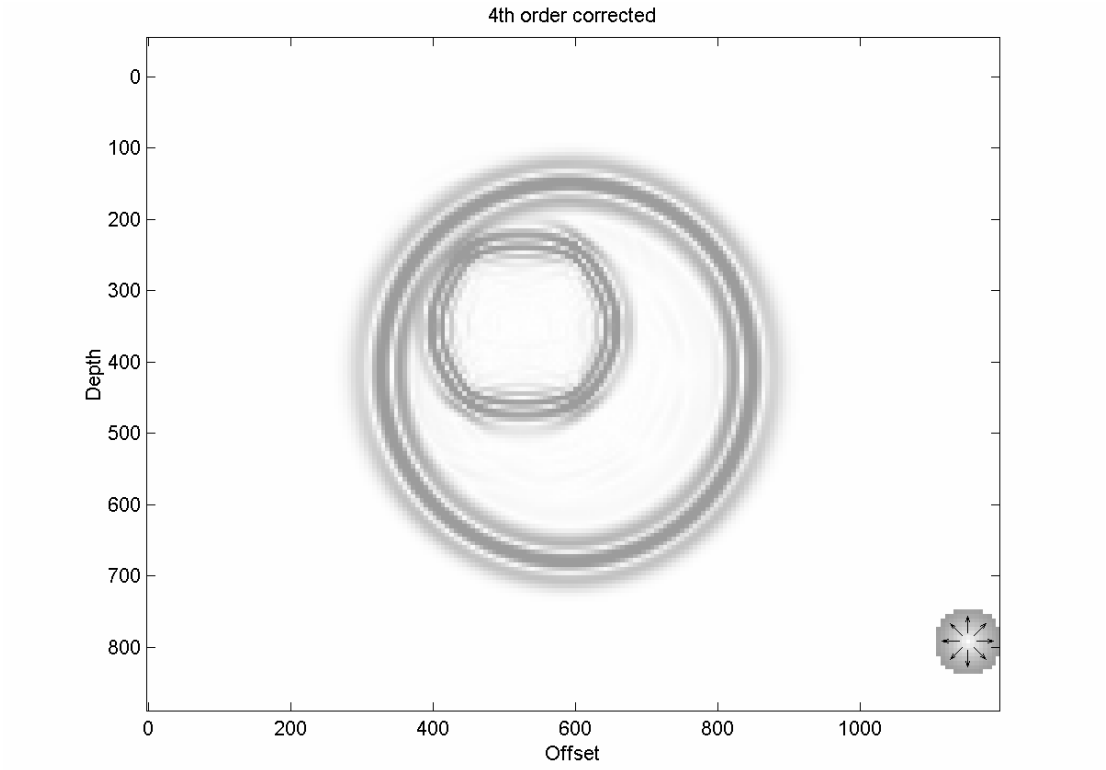

FIG. 20: The model using 4th order accurate 2nd spatial derivatives. Compare with Figure 19.

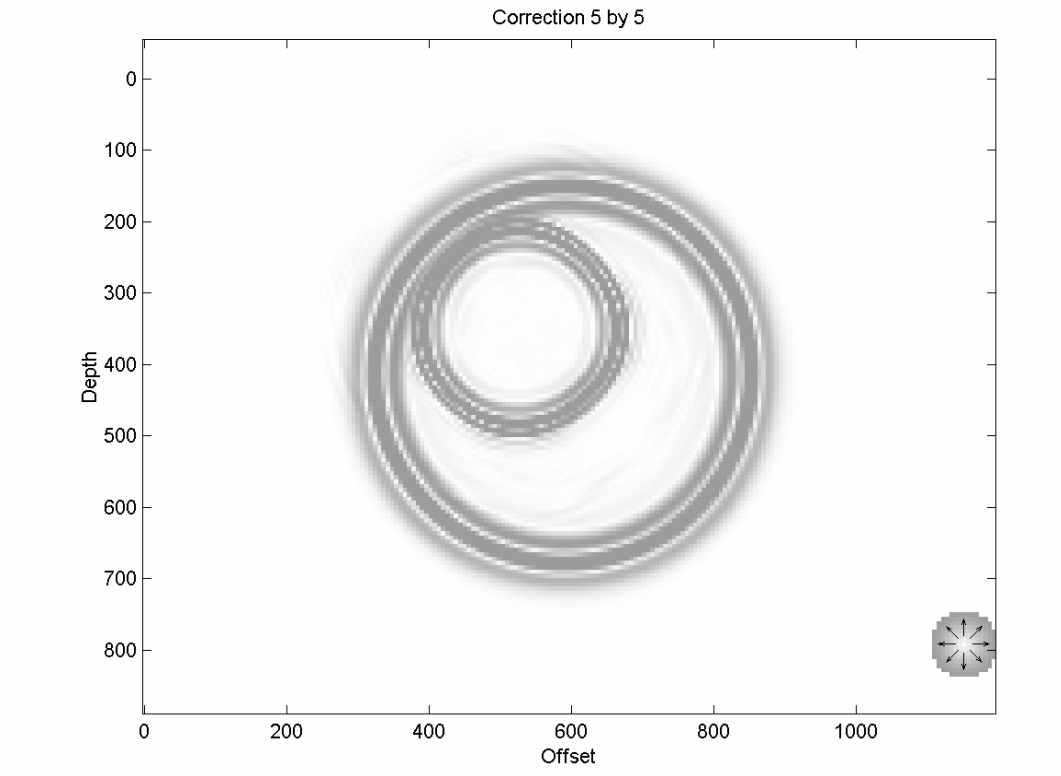

FIG. 21: The model with corrections limited to a 5 by 5 spatial filter. Compare with Figure 20.

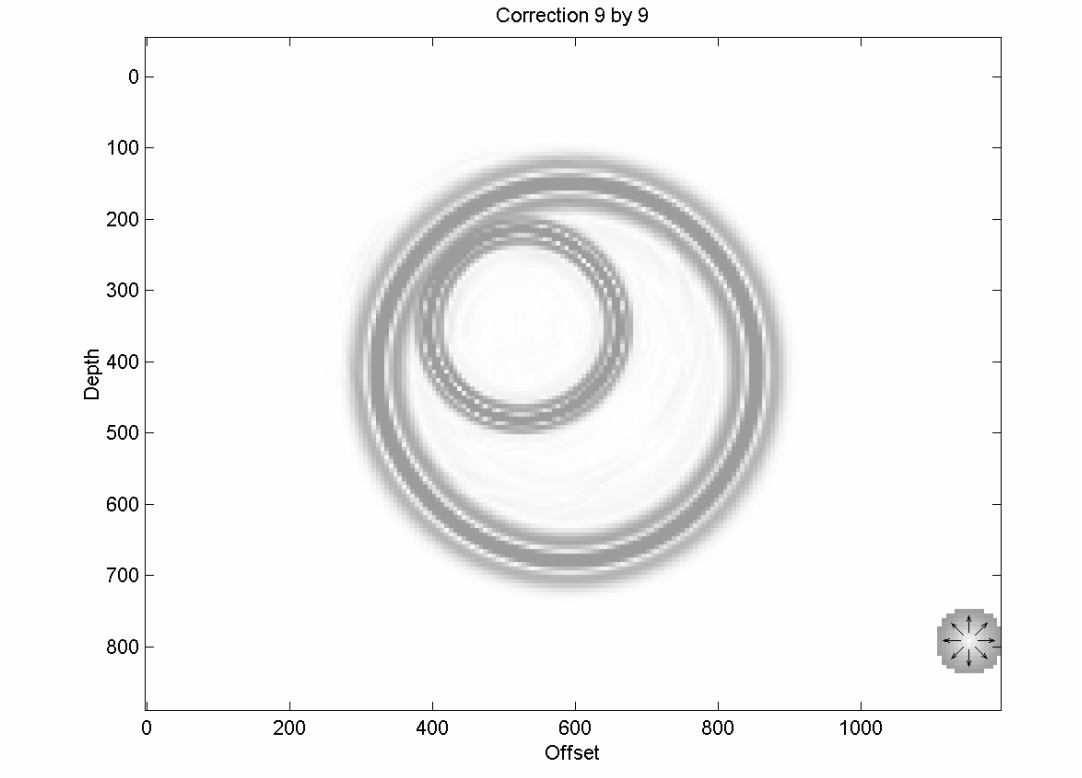

FIG. 22: The model with corrections of a 9 by 9 spatial filter. Compare with Figure 21.